

# Photometric variability of the LAMOST sample of magnetic chemically peculiar stars as seen by TESS<sup>★</sup>

J. Labadie-Bartz<sup>1,2,3</sup>, S. Hümmerich<sup>4,5</sup>, K. Bernhard<sup>4,5</sup>, E. Paunzen<sup>6</sup>, and M. E. Shultz<sup>7</sup>

<sup>1</sup> LESIA, Paris Observatory, PSL University, CNRS, Sorbonne University, Université Paris Cité, 5 place Jules Janssen, 92195 Meudon, France

<sup>2</sup> Instituto de Astronomia, Geofísica e Ciências Atmosféricas, Universidade de São Paulo, Rua do Matão 1226, Cidade Universitária, B-05508-900 São Paulo, SP, Brazil

<sup>3</sup> Homer L. Dodge Department of Physics and Astronomy, University of Oklahoma, 440 W. Brooks Street, Norman, OK 73019, USA

<sup>4</sup> Bundesdeutsche Arbeitsgemeinschaft für Veränderliche Sterne e.V. (BAV), Berlin, Germany

<sup>5</sup> American Association of Variable Star Observers (AAVSO), Cambridge, USA

<sup>6</sup> Faculty of Science, Masaryk University, Department of Theoretical Physics and Astrophysics, Kotlářská 2, 611 37 Brno, Czechia

<sup>7</sup> Department of Physics and Astronomy, University of Delaware, 217 Sharp Lab, Newark, Delaware 19716, USA

## ABSTRACT

**Context.** High-quality light curves from space-based missions have opened up a new window on the rotational and pulsational properties of magnetic chemically peculiar (mCP) stars and have fuelled asteroseismic studies. They allow the internal effects of surface magnetic fields to be probed and numerous astrophysical parameters to be derived with great precision.

**Aims.** We present an investigation of the photometric variability of a sample of 1002 mCP stars discovered in the Large Sky Area Multi-Object Fiber Spectroscopic Telescope (LAMOST) archival spectra with the aims of measuring their rotational periods and identifying interesting objects for follow-up studies.

**Methods.** Transiting Exoplanet Survey Satellite (TESS) data were available for 782 mCP stars and were analysed using a Fourier two-term frequency fit to determine the stars' rotational periods. The rotational signal was then subtracted from the light curve to identify additional non-rotational variability signals. A careful pixel-level blending analysis was performed to check whether the variability originates in the target star or a nearby blended neighbour. We investigated correlations between the observed rotational periods, fractional age on the main sequence, mass, and several other observables.

**Results.** We present rotational periods and period estimates for 720 mCP stars. In addition, we have identified four eclipsing binary systems that likely host an mCP star, as well as 25 stars with additional signals consistent with pulsation (12 stars with frequencies above  $10 \text{ d}^{-1}$  and 13 stars with frequencies below  $10 \text{ d}^{-1}$ ). We find that more evolved stars have longer rotation periods, which is in agreement with the assumption of the conservation of angular momentum during the main-sequence evolution.

**Conclusions.** With our work, we increase the sample size of mCP stars with known rotation periods and identify prime candidates for detailed follow-up studies. This enables two paths towards future investigations: population studies of even larger samples of mCP stars and the detailed characterisation of high-value targets.

**Key words.** stars: chemically peculiar – stars: rotation – techniques: photometric – stars: binaries: eclipsing – stars: oscillations (including pulsations)

## 1. Introduction

The chemically peculiar (CP) stars of the upper main sequence form a significant fraction of the upper main-sequence stars (about 10 per cent) and are encountered between spectral types early B to early F. Their defining characteristic is the presence of spectral peculiarities that indicate unusual elemental abundance patterns (e.g. Preston 1974; Maitzen 1984; Smith 1996; Gray & Corbally 2009; Ghazaryan et al. 2018), which are thought to originate from the interplay between radiative levitation and gravitational settling taking place in the calm outer layers of slowly rotating stars (atomic diffusion; e.g. Michaud 1970; Richer et al. 2000).

Following Preston (1974), the four main groups of CP stars are the CP1 stars (the metallic-line or Am/Fm stars), the CP2 stars (the magnetic Bp/Ap stars), the CP3 stars (the mercury-

manganese or HgMn stars), and the CP4 stars (the He-weak stars). Although the observed abundance patterns within a group can vary considerably, each group is characterised by a distinct set of peculiarities. The CP1 stars exhibit under-abundances of Ca and Sc and over-abundances of iron-peak and heavier elements. The main characteristics of the CP2 stars are excesses of elements such as Si, Sr, Eu, or the rare-earth elements. Some of the most peculiar objects belong to this group, such as the extreme lanthanide star HD 51418 (Jones et al. 1974) or Przybylski's Star, HD 101065 (Przybylski 1966). The CP3 stars show enhanced lines of Hg and Mn and other heavy elements, whereas the CP4 stars possess anomalously weak He lines. Additional classes of CP stars have been proposed, for example the  $\lambda$  Bootis stars (Gray 1997; Paunzen 2004; Murphy & Paunzen 2017), which are characterised by unusually low surface abundances of iron-peak elements, or the He strong stars, which are early B stars that exhibit anomalously strong He lines in their spectra (Bidelman 1965; Morgan et al. 1978). As regards the strength of

\* Table A.1 is available in electronic form at the CDS via anonymous ftp to cdsarc.cds.unistra.fr (130.79.128.5) or via <https://cdsarc.cds.unistra.fr/cgi-bin/qcat?J/A+A/>

chemical peculiarities, a continuous transition from chemically normal to CP stars is observed (Loden & Sundman 1987).

Several authors have divided the CP stars into a ‘magnetic’ and a ‘non-magnetic’ sequence (e.g. Preston 1974; Maitzen 1984). The former is made up of the CP2 and the He-peculiar stars (i.e. the CP4 and the He-strong stars), which possess strong and stable magnetic fields, while the latter encompasses, for example, the CP1, CP3, and  $\lambda$  Bootis stars. While this canonical view has been frequently challenged (cf. e.g. Hubrig et al. 2010, 2012; Kochukhov et al. 2013, and Hubrig et al. 2020 on the ongoing controversy about the presence of weak and tangled magnetic fields in CP3 stars), the groups of stars of the non-magnetic sequence certainly lack the strong and organised magnetic fields observed in the CP2 and He-peculiar stars, which can attain strengths of up to several tens of kilogauss (Babcock 1947; Aurière et al. 2007). For convenience, CP2 and He-peculiar stars are generally referred to as magnetic chemically peculiar (mCP) stars – a convention that we adhere to in this study.

While the origin of their magnetic fields is still a matter of some controversy (Moss 2004), evidence has been collected in favour of the fossil field theory (e.g. Braithwaite & Spruit 2004), according to which the magnetic field is a relic of the interstellar magnetic field that was ‘frozen’ into the stellar plasma during star formation. Alternatively, a fossil field may be generated during a merger event (e.g. Tutukov & Fedorova 2010; Schneider et al. 2019).

Magnetic CP stars show a non-uniform surface distribution of chemical elements, which is associated with the presence of the magnetic field and manifests itself in the formation of spots and patches of enhanced or depleted element abundance. Flux is redistributed in these ‘chemical spots’ (line and continuum blanketing; e.g. Wolff & Wolff 1971; Molnar 1973; Lanz et al. 1996; Shulyak et al. 2010; Krčíká et al. 2013), and mCP stars show strictly periodic light, spectral, and magnetic variations with the rotation period, which are satisfactorily explained by the oblique-rotator model (the magnetic axis is oblique to the rotation axis; Stibbs 1950). According to convention, photometrically variable mCP stars are referred to, after their bright prototype, as  $\alpha^2$  Canum Venaticorum (ACV) variables (Samus et al. 2017). Rotation periods generally range from about 0.5 days to decades, with a peak at  $\sim$ 2 days (e.g. Renson & Manfroid 2009; Bernhard et al. 2015a).

In addition to the rotational light changes, mCP stars can also exhibit pulsational variability. For a long time, the only proven form of pulsational variability among these objects was observed in the so-called rapidly oscillating Ap stars (Kurtz 1982), which exhibit variability in the period range 5–20 min (high-overtone, low-degree, and non-radial pulsation modes). With the advent of ultra-precise space photometry, additional pressure modes (p modes) and gravity modes (g modes) associated with  $\gamma$  Doradus (e.g. Kaye et al. 1999; Guzik et al. 2000) and  $\delta$  Scuti (e.g. Breger 2000) pulsations were identified in a number of CP2 stars (e.g. Balona et al. 2011; Cunha et al. 2019; Holdsworth et al. 2021). In general, the high-quality light curves (LCs) from space-based missions open up the possibility for the asteroseismic characterisation of mCP stars, which in turn allows the internal effects of surface magnetic fields to be probed and numerous astrophysical parameters to be derived with great precision (Briquet et al. 2012; Buyschaert et al. 2018).

The most up-to-date collection of CP stars is the General Catalogue of CP Stars (Renson & Manfroid 2009), which was published more than a decade ago. It lists about 3500 mCP stars or candidates ( $\sim$ 2000 confirmed mCP stars and  $\sim$ 1500 candidates) and is still one of the main resources regularly employed

in investigations of mCP stars. However, in recent years, several studies have published new samples of these objects (e.g. Hümerich et al. 2018; Scholz et al. 2019; Sikora et al. 2019a). Of note is the study of Hümerich et al. (2020, hereafter Paper 1), who published a sample of 1002 mCP stars, thereby significantly enlarging the total known number of these objects.

Here we present our efforts to characterise the photometric variability of the sample of mCP stars published in Paper 1 using photometric time-series observations from the NASA Transiting Exoplanet Survey Satellite (TESS; Ricker et al. 2015). Our paper is structured as follows. The employed data sources and methods are described in Sect. 2. In Sect. 3 we present and discuss our results. Special emphasis is placed on the eclipsing binary (EB) systems and pulsator candidates in our sample, which are studied in detail in Sect. 4. We conclude in Sect. 5.

## 2. Methods and data

### 2.1. The LAMOST DR4 sample of mCP stars

In our search for mCP stars (Paper 1), we employed a modified version of the MKCLASS code<sup>1</sup>, a computer program conceived by Richard O. Gray to classify stellar spectra on the MK system, to search for mCP stars in spectra from the fourth data release (DR4) of the Large Sky Area Multi-Object Fiber Spectroscopic Telescope (LAMOST) of the Chinese Academy of Science (Zhao et al. 2012; Cui et al. 2012). LAMOST is a Schmidt telescope based at Xinglong Observatory (Beijing, China) that boasts an effective aperture of 3.6–4.9 m (field of view of about 5°) and is able to collect 4000 spectra in a single exposure (spectral resolution  $R \sim 1800$ , limiting magnitude  $r \sim 19$  mag, wavelength coverage 3700 to 9000 Å). LAMOST is therefore perfectly suited for large-scale spectral surveys; data products are made available to the public in consecutive data releases accessible through the LAMOST spectral archive.<sup>2</sup>

In a nutshell, suitable candidates were collected from a colour-selected sample of early-type stars by searching for the presence of the 5200 Å flux depression, a characteristic of mCP stars (e.g. Kodaira 1969; Maitzen 1976; Paunzen et al. 2005; Kochukhov et al. 2005; Khan & Shulyak 2006). Spectral classification was then performed using MKCLASS\_mCP, a version of the original program modified to probe a number of spectral features relevant to the identification and classification of mCP stars. In this way, a final sample of 1002 mCP stars (mostly CP2 stars and several CP4 stars) was collected, most of which were new discoveries (only 59 objects have an entry in the Renson & Manfroid (2009) catalogue). These objects are between 100 Myr and 1 Gyr old, with the majority having masses between  $2 M_{\odot}$  and  $3 M_{\odot}$ . From an investigation of a sub-sample of 903 mCP stars with accurate astrophysical parameters, we determine a mean fractional age on the main sequence of  $\tau = 63\%$  (standard deviation of 23 %) and conclude that our results provide evidence for an inhomogeneous age distribution among low-mass ( $M < 3 M_{\odot}$ ) mCP stars. For more detailed information on the methods employed, we refer the reader to Paper 1.

### 2.2. TESS data

The NASA TESS mission was launched in 2018 with the primary goal of discovering transiting exoplanets via high-precision time-series photometry. The four identical cameras of

<sup>1</sup> <http://www.appstate.edu/~grayro/mkclass/>

<sup>2</sup> <http://www.lamost.org>



coarsely estimated (cf. also Sect. 3.1). In some cases, it was not possible to determine or even estimate a rotational period from the TESS data (e.g. when the rotation period was too long, the amplitude too small, or the data problematic).

A given star in our sample may also display non-rotational photometric variability due to, for example, stochastic low-frequency excess (astrophysical correlated red noise, Bowman et al. 2019, 2020), pulsation, binarity, or a combination thereof. To investigate this, a two-term model of the rotational modulation was subtracted from the LC, whereafter the standard (one-term) frequency spectrum was calculated, which was then fit to determine the red noise profile (similar to the method used by Bowman et al. 2020; Labadie-Bartz et al. 2021). The red noise profile, multiplied by 5, was then used as a threshold above which other statistically significant frequencies (in general not associated with the stellar rotation from the first step) were automatically identified as candidates with additional variability. This step led to the identification of 107 such candidates.

However, given the large pixel size of TESS (21 arcseconds), contaminating flux from neighbouring stars falling into the aperture ('blending') is a concern. Therefore, LCs were re-extracted for these candidates including up to the most recent Cycle 5 images for a pixel-level blending analysis. This was done in two steps. The first 'coarse' analysis involved marking the location of all nearby *Gaia* sources (with  $G_{\text{mag}} < 15$ ) overlaid on an image of the TESS TPF, and plotting the LC and frequency spectrum of each pixel in the vicinity of the target and then comparing the per-pixel frequency spectrum to that calculated from the PCA-detrended LC for the target star. In this way, candidate pulsational signals (or other variabilities) could be localised to determine if they originate in or near the target star or in a nearby blended neighbour. A suite of plots were inspected manually to make this determination. This analysis was generally sufficient to identify variable sources  $\sim 2$  or more pixels away from the mCP target star. Each object that passed this first analysis was then examined in more detail using the TESS\_LOCALIZE<sup>3</sup> Python package (Higgins & Bell 2022). TESS\_LOCALIZE is designed to locate the origin of variability signals to within one-fifth of a TESS pixel. In all objects analysed with TESS\_LOCALIZE, the rotational variability was confirmed to originate in the mCP star, and two objects with additional frequencies were rejected as blends (in both these cases the blended variable was faint,  $G_{\text{mag}} \sim 17$  to 18, and about one pixel away from the mCP star).

Each star determined to potentially have inherent variability in addition to rotation is listed in Sect. 4. Those objects with additional variability due to contaminating flux from blended neighbouring sources are indicated (see Sect. 3.1) in order to minimise duplication of efforts in future studies. We note that the typically low-amplitude signals from blended neighbours do not impact the analysis of the rotational variability of these objects – no cases were identified where the presumed rotational modulation originates off-target.

### 3. Results and discussion

#### 3.1. Presentation of results

Table A.1 in the appendix lists essential data for our sample stars, including identifiers from the TESS Input Catalogue (TIC; Stassun et al. 2019) and LAMOST; positional information and magnitude in the  $G$  band from *Gaia* DR3 (Gaia Collaboration et al. 2016; Babusiaux et al. 2022; Gaia Collaboration et al. 2022);

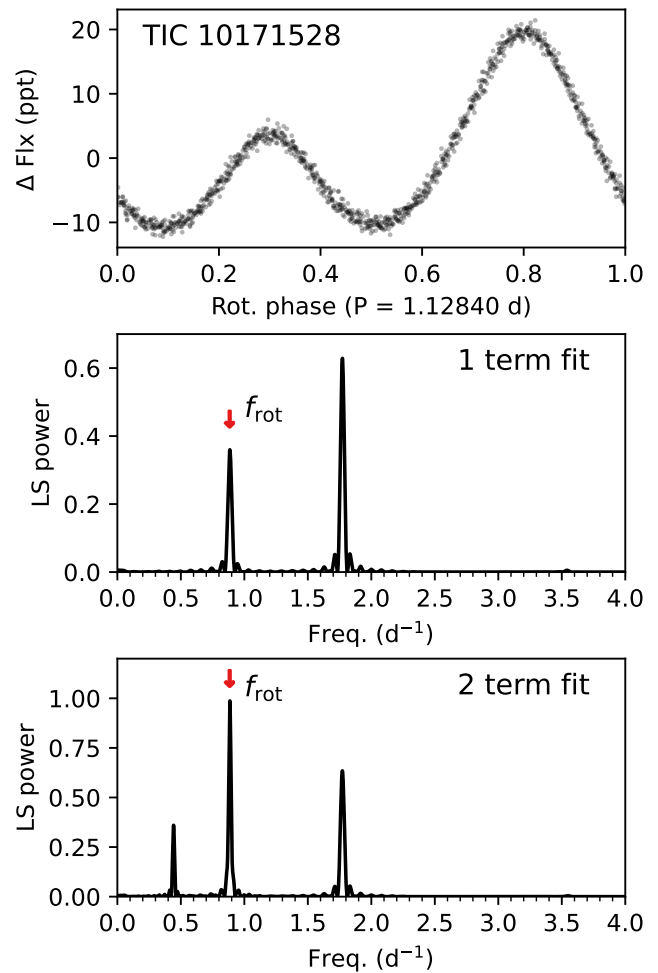


**Fig. 1.** Comparison of one- and two-term Fourier analysis for identifying the rotation period. *Top*: Phased TESS LC for an example mCP star with a decidedly double-waved pattern at the rotational period (i.e. two maxima and two minima per rotation). *Middle*: Standard single-term frequency analysis, showing that the strongest peak is at  $2 \times f_{\text{rot}}$ . *Bottom*: Two-term frequency analysis, where the strongest peak is at  $f_{\text{rot}}$ .

spectral type from Paper 1; and variability period and peak-to-peak amplitude, as derived from TESS data in this study. Where appropriate, additional information is provided in the column 'Remarks', which includes variability information gleaned from the International Variable Star Index of the AAVSO (VSX; Watson 2006). The VSX is the most up-to-date collection of variable star data and constantly updated with new variability catalogues and results from the literature. It contains the results of most relevant papers dealing with the periods of ACV variables (including more recent studies, such as Paunzen & Maitzen 1998, Wright et al. 2012, Bernhard et al. 2015a, Bernhard et al. 2015b, Hümerich et al. 2016, and Bernhard et al. 2021). Not included at the time of this writing are the studies of Bowman et al. (2018), Sikora et al. (2019a), David-Uraz et al. (2019), Bernhard et al. (2020), Mathys et al. (2020b), and Mathys et al. (2022). Except

<sup>3</sup> <https://github.com/Higgins00/TESS-Localize>

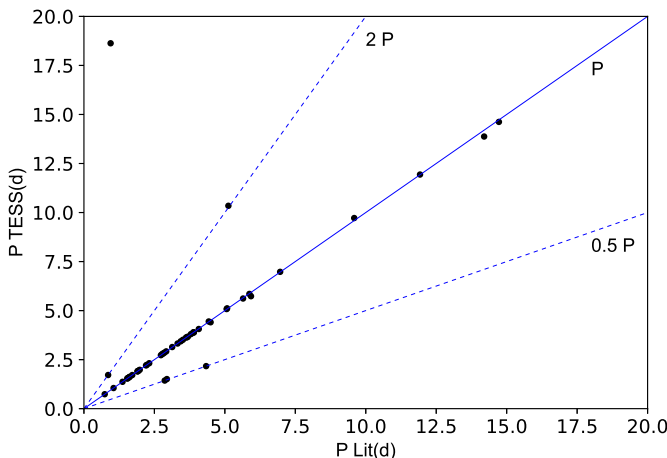


**Fig. 2.** Comparison of literature periods and periods derived from the analysis of TESS data in this work for the 64 stars with periods listed in the VSX. The outlying data point refers to TIC 237662091, which is discussed in the text.

for two stars from the list of Mathys et al. (2022)<sup>4</sup>, there are no matches between the samples of these studies and our sample.

The VSX has data for only 64 out of the 782 objects presented here. With the present work, we therefore significantly add to the sample of mCP stars with accurately determined rotational periods. We note that for several objects, the VSX designations are not accurate (although the periods may still be correct), for example when variability was interpreted as being related to binarity and not rotation or when the object was included under a generic variability type such as ROT or MISC. These objects are here identified as ACV variables for the first time.

Figure 2 illustrates a comparison of the literature periods from the VSX with the periods derived from TESS data in this work. In five cases, the period values in the VSX obviously represent half (TIC 235273014, TIC 2679119) or twice (TIC 438165498, TIC 250478934, TIC 21018674) the true rotation period. This is expected, as double-waved ACV LCs can easily be misinterpreted as single-waved LCs (or vice versa) if the data are noisy, the amplitude of the light variations is very small, or the difference in brightness between both maxima or minima is negligible. In this respect, the ultra-precise TESS data clearly have an advantage over ground-based photometric data sources for typical periods. Apart from that, the agreement is very good, which highlights the quality of the VSX period data. The single exception is for TIC 237662091, where TESS clearly revealed a long rotation period (18.630 d, although it is possible the true rotation period is twice this value), and the VSX period corresponds to the daily alias (0.94661 d).

Periods are given to the last significant digit. Approximate periods are identified by the use of a colon (':'). Several stars are clearly variable but have periods too long to be resolved with the rather short time baseline of the employed TESS data. That is expected, as ACV variables can have periods of up to decades or even longer (Mathys 2019; Mathys et al. 2019, 2020a,b, 2022). These objects are identified by the remark ‘long-period var.’ in Table A.1. We caution that it is not always straightforward to distinguish between long-term trends inherent to the TESS data

and intrinsic stellar variability, in particular when the data are noisy. Therefore, a question mark is added to the aforementioned remark when the situation remains unclear.

Most of these suspected long-period ACV variables boast data from one sector only (time baseline of 27 days) so that not more than a part of the rotational cycle was covered in the available data. These objects are consequently listed with a period of “>30:” in Table A.1. Two examples of stars with periods longer than a single TESS sector are shown in Fig. 3, which also illustrates the difficulties encountered in period determination for these objects even when data from several sectors are available. Since each sector is reduced separately, there are different systematic trends and different amounts of contaminating flux from neighbouring stars, so the measured photometric amplitude can differ from one sector to the next, and different constant flux offsets may need to be applied to each sector of data (or even each half-sector; to avoid discontinuities). For stars such as these, the background-corrected version of the LC typically produces better results (as plotted here) since the PCA detrending tends to remove or distort the longer-term signals (see Sect. 2.3).

In 62 stars, no variability could be inferred from TESS data. For 23 of these objects, a LC of reasonable or good quality is extracted, yet no variability is seen (remark ‘data fine, no var.’). We consider these stars prime candidates for very slowly rotating mCP stars. One of these objects (TIC 239801694) has been proposed to be a very slowly rotating mCP star candidate by Mathys et al. (2022).

For the remaining objects, blending issues or problems with either the LC extraction or detrending yield unreliable results. Some of these stars do not fall on useful pixels on the TESS CCD, and thus no LC could be extracted (remark ‘edge of CCD, no LC extracted’). Other targets are faint and in a relatively crowded field and so the automatic aperture selection failed (remark ‘faint, aperture selection failed’), or there is significant blending from (often relatively bright) neighbouring sources, rendering it difficult or impossible to isolate the target star (remark ‘blending dominates, LC unreliable’). Finally, in some LCs there are problems in detrending against systematic effects making it difficult to determine whether or not there is any astrophysical variability (‘systematics dominate, LC unreliable’).

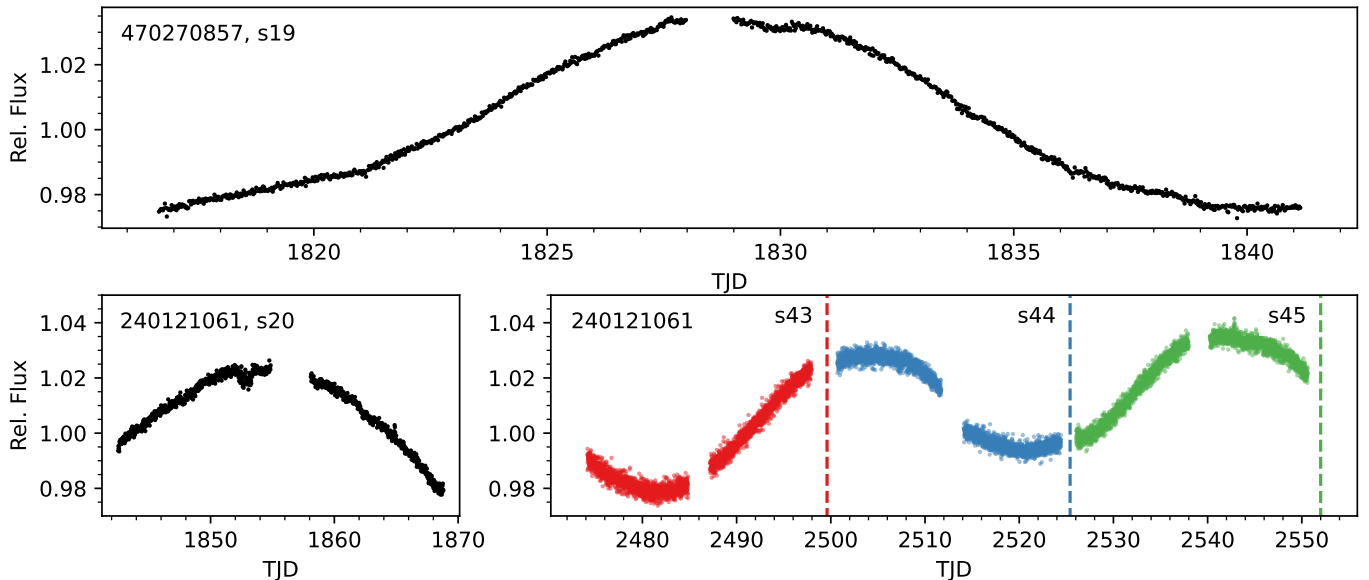
Stars of special interest, which are further discussed in Sect. 4, are marked by an asterisk (\*) in the column ‘Remarks’. These are the EBs (Sect. 4.1) and stars with additional signals that we attribute to pulsation (or in some cases where these additional signals have a harmonic structure to perhaps rotation or binarity of an unresolved object; Sect. 4.2). In regard to the pulsator candidates, corresponding remarks identify whether additional signals in the low-frequency (<10 d<sup>-1</sup>; ‘add. low-freq. signal’) or high-frequency (>10 d<sup>-1</sup>; ‘add. high-freq. signal’) realms were detected.

The LCs of several objects clearly show eclipses or other additional variability that a pixel-level blending analysis revealed to originate in a neighbouring star in close proximity on the sky (cf. Sects. 2.5 and 4.1). These objects are identified by the remark ‘eclipses not on target’ and ‘add. var. not on target’, respectively, in Table A.1, mainly to avoid confusion in further studies dealing with these stars.

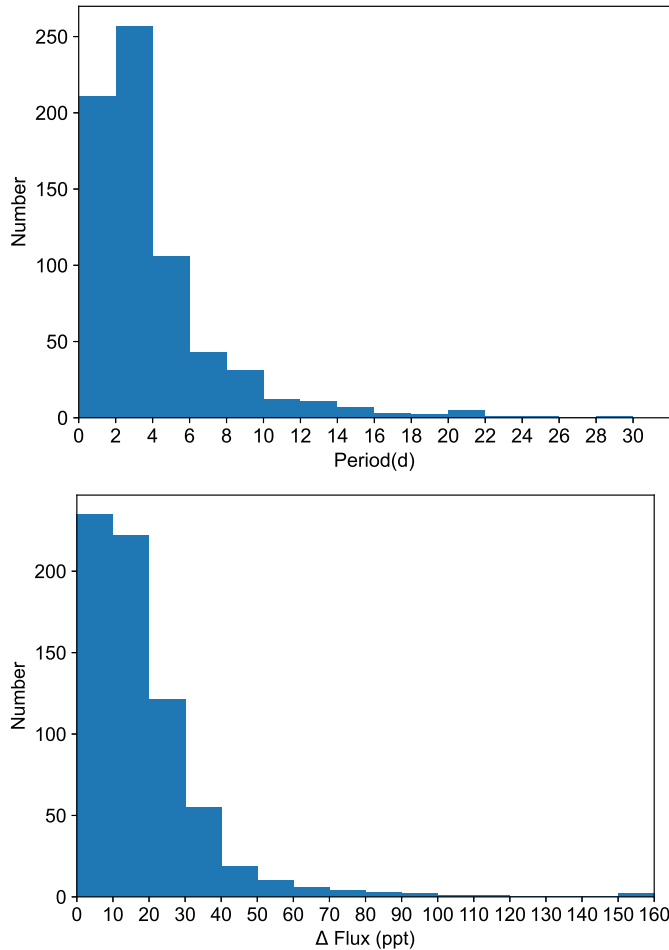
### 3.2. Rotation period versus fractional age on the main sequence and stellar mass

Figure 4 investigates the distribution of rotation periods (upper panel) and the photometric peak-to-peak amplitudes in the TESS bandpass (lower panel) of the 720 sample stars for which these

<sup>4</sup> Mathys et al. (2022) identified TIC 239801694 and TIC 368073692 as candidate very slowly rotating mCP stars; no variations were reported. Our analysis also found no variations in TIC 239801694, but for TIC 368073692 we found a period of 20.49 d with a consistent signal in both available sectors of data.



**Fig. 3.** Two stars with periods longer than a single TESS sector. For TIC 470270857 (top), only one sector of data was available. For TIC 240121061, one sector in Cycle 2 and three consecutive sectors in Cycle 4 were available. Even with three sectors, the rotation period is difficult to determine – it may be  $\sim 40$  days (if single-waved) or  $\sim 80$  days (if double-waved).



**Fig. 4.** Histograms of the distribution of rotational periods (upper panel) and photometric peak-to-peak amplitudes in the TESS bandpass (lower panel) of the 720 sample stars for which these parameters could be derived.

parameters could be derived from TESS data. Our results are in excellent agreement with the literature and illustrate the well-known peak around  $P_{\text{rot}} \sim 2$  days (e.g. Renson & Manfroid 2009; Bernhard et al. 2015a,b; Hümmerich et al. 2016; Sikora et al. 2019b) and the typical magnitude range of the photometric variations (e.g. Manfroid & Mathys 1986; Bernhard et al. 2015a) that appear somewhat reduced in the broad red bandpass of the TESS mission (600–1000 nm; cf. Bernhard et al. 2020).

The correlations between the derived rotation periods with the fractional age on the main sequence ( $\text{Tau}$ ) and the stellar mass ( $M$ ) are illustrated in Fig. 5.  $\text{Tau}$  and  $M$  values are taken from Paper 1. We find a correlation in the sense that more evolved stars have longer rotation periods, which is in agreement with results from the literature that confirmed that the evolution of rotation periods among mCP stars agrees very well with the assumption of conservation of angular momentum during the main-sequence evolution (cf. e.g. the discussion in Adelman 2002; Netopil et al. 2017). Magnetic braking is well known to spin down magnetic B stars as they evolve (Shultz et al. 2019b), and could also be a factor in the trend observed in our mCP sample of slower rotation with age. However, it is generally suggested that magnetic braking is weak in mCP stars and that the primary reason for spin-down is changes of the moment of inertia (with angular momentum conserved; North 1998; Kochukhov & Bagnulo 2006).

Apparently, there is no correlation between rotation period and mass. The stars with no detected rotational variability (presumed to be very slow rotators) have a similar distribution of age compared with the majority of the sample where a rotation period is determined, but may preferentially have lower masses. However, with only 23 very slow rotator candidates, the sample is too small to draw any statistical conclusions.

While our results lend themselves perfectly for further statistical analyses, these are out of scope of this study and are best investigated with as large a sample of mCP stars as possible. This will be the topic of an upcoming paper (Paunzen et al., in preparation). Nevertheless, some preliminary findings on the

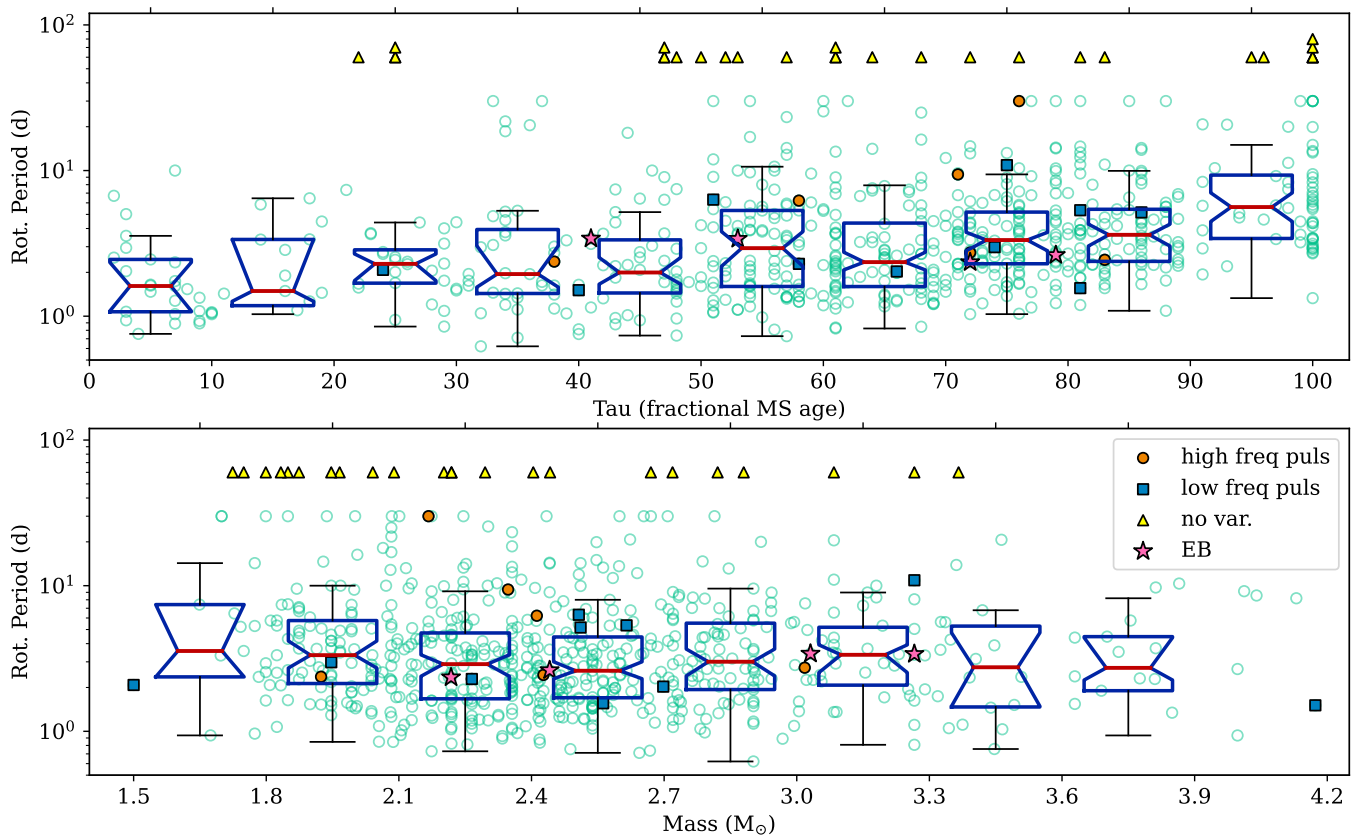


**Fig. 5.** Derived rotation period from TESS versus the fractional main-sequence age ( $\text{Tau}$ , expressed as a percentage; upper panel) and stellar mass (lower panel). Data were binned, with the overlaid box plots extending from the lower to upper quartile values and the horizontal red line representing the median. The notches in the box indicate the 95% confidence interval of the median, and the whiskers extend to the limits of the binned data, excluding the statistical outliers. In the bottom panel, the first bin includes masses less than  $1.8 M_{\odot}$ , and the last bin all masses greater than  $3.6 M_{\odot}$ . Otherwise, the mass bins are  $0.3 M_{\odot}$  wide. There is a correlation with more evolved stars having longer rotation periods, but there is apparently no correlation with the mass. Stars with additional high-frequency ( $>10 \text{ d}^{-1}$ ) or low-frequency ( $<10 \text{ d}^{-1}$ ) signals are indicated by the orange circles and blue squares, respectively (not all of them have stellar parameters from Paper 1). Yellow triangles mark the 23 stars where no variability was detected (and we could not measure a rotation period), which are candidate very slow rotators. Stars with estimated rotation periods of “ $>30$ ” (i.e. slow but detectable rotational variability longer than a single TESS sector, as in Fig. 3) are included in this plot with  $P_{\text{rot}} = 30 \text{ d}$  as a lower limit. The four EBs are marked by pink stars, but their mass and age may not be accurate since their binarity was not considered in Paper 1.

correlations between several observables are shortly discussed in Sect. B.

#### 4. Note on special objects

##### 4.1. Eclipsing binaries

Four systems are found to be EBs. Many additional targets contain eclipses in the extracted LCs, but a pixel-level blending analysis (Sect. 2.5) shows that the eclipses originate in a neighbouring star. These four EBs are listed and briefly described below and are shown in Fig. 6. EBs containing CP stars are rare and are valuable opportunities for precise determinations of the stellar and system properties (e.g. Kochukhov et al. 2021). Among the hot stars on the upper main sequence, global magnetic fields are found in about 10% of effectively single stars, but only in 2% of close binaries (Alecian et al. 2015). Discovering and characterising EBs which host magnetic stars are important for constraining the origin of magnetism in hot stars (e.g. Shultz et al. 2019a).

TIC 2941395 (= UCAC4 624-023360,  $V_{\text{mag}} = 13.5$ ): The rotational signal is not in phase with the eclipses – that is, the rotation and binary periods are not identical, with the mCP star

apparently rotating slower than the orbit. A frequency analysis was performed after clipping out all eclipses to derive a rotation period of  $P_{\text{rot}} = 2.346688 \text{ d}$  ( $f_{\text{rot}} = 0.426132 \text{ c/d}$ ). The orbital period is  $P_{\text{orb}} = 1.6815 \text{ d}$  ( $f_{\text{orb}} = 0.5947 \text{ c/d}$ ). At such short orbital periods, synchronisation is expected, perhaps casting doubt that the mCP star is involved in the eclipsing system as in, for example, a hierarchical triple system with an inner EB and an outer mCP star. This has not previously been reported as an EB.

TIC 39818458 (= HD 40759,  $V_{\text{mag}} = 9.3$ ): This is an EB, with eclipses on-target, and is included in the TESS OBA EB catalogue of IJspeert et al. (2021). There appears to be variability caused by three different scenarios – rotation, pulsation, and orbital. In addition to the clearly visible slower pulsation (consistent with g-modes), there are also many higher-frequency  $\delta$  Scuti-like pulsation modes (between  $\sim 50 - 60 \text{ d}^{-1}$ ). All eclipses are the same depth (i.e. there is no visible secondary eclipse) and are not flat-bottomed, occurring every 3.8155 days. The rotational period of the mCP star is determined to  $P_{\text{rot}} = 3.3949695 \text{ d}$ . This system is being characterised in more detail by Semenko et al., in prep, and so is not discussed further in this work.



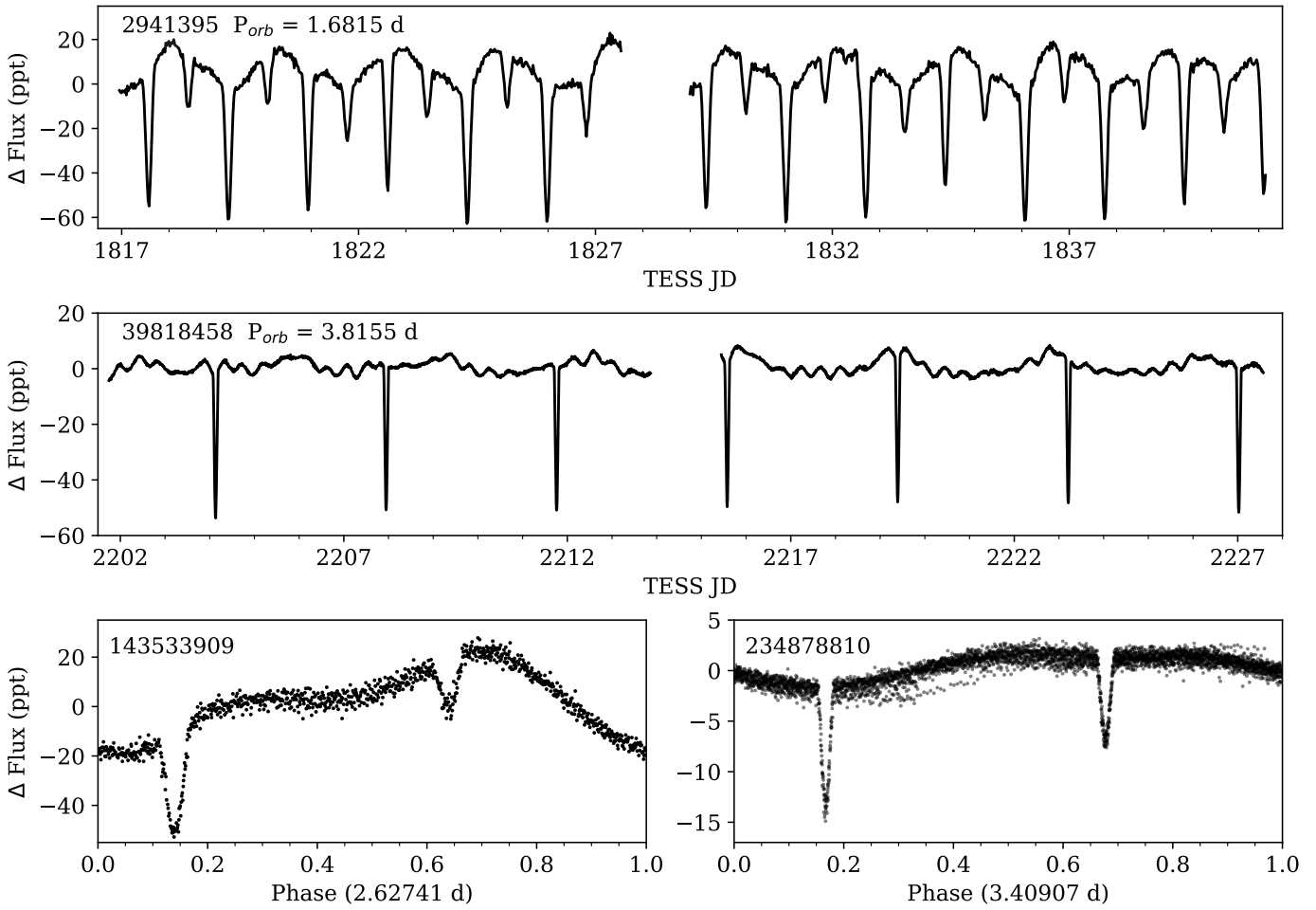


**Fig. 6.** LCs of the four EBs identified in the sample. In the top two panels, a single sector of TESS data is shown, un-phased (since neither the rotational nor pulsational signals are synchronised to the binary orbit). The bottom two panels are phased to the rotational periods, which are identical to the orbital periods. TIC identifiers are indicated in each panel.

TIC 427377135 (= HD 36955,  $V_{\text{mag}} = 9.58$ ): There are multiple high-frequency signals between  $31$  and  $55 \text{ d}^{-1}$  (plus one near  $19 \text{ d}^{-1}$ ), all of which originate on-target. SIMBAD lists this as a ‘Double or Multiple star’, probably due to the object being listed in the Washington Visual Double Star Catalog (Mason et al. 2001) where the secondary is ‘probably early-K’ and is  $1.5$  arcsec distant. However, all *Gaia* sources within  $1$  arcminute are fainter than the 16th magnitude (the closest, at  $13$  arcsec, is  $G_{\text{mag}} = 21$ ), casting doubt on this star being a visual double, and there is no indication of blending from some neighbouring source in the TESS images. The rotation frequency of the mCP star is  $0.43765 \text{ d}^{-1}$ . There are three additional low-frequency signals unrelated to this rotation frequency. The strongest is at  $0.56546 \text{ d}^{-1}$ , and the next two are at slightly below two and three times this, almost, but not quite, forming a harmonic series, which suggests the signals are probably not related to rotation or binarity (see Fig. 8). These signals may be consistent with a sequence of g modes, as in the  $\gamma$  Dor pulsators. The higher-frequency signals are numerous and seemingly unrelated to these lower frequencies, and are probably indicative of  $\delta$  Scuti pulsation.

TIC 431659618 (TYC 4001-1858-1,  $V_{\text{mag}} = 10.75$ ): There is perhaps a significant frequency at about  $11.8 \text{ d}^{-1}$ , which seems to originate on-target (amplitude  $\sim 0.5 \text{ ppt}$ ). However, this is located within a broader ‘bump’ in the frequency spectrum that may be due to some unidentified systematic effect in the data.

TESS\_LOCALIZE finds rotation on-target, but cannot locate the higher-amplitude signal (perhaps hinting at its origin in systematics).

#### 4.2.2. Lower-frequency ( $< 10 \text{ d}^{-1}$ ) signals

In addition to the stars with higher-frequency signals (some of which also exhibit lower-frequency signals in addition to the mCP rotation), there are 13 stars with low-frequency signals that are not harmonics of the main rotation frequency. In most of these, pulsation is likely, but in others the additional signals seem more consistent with binarity or the rotation of an unresolved source that is not the mCP star (i.e. when the signals have a harmonic structure like for TIC 34366540, 252325936, 268376046, and 403748236). The TESS frequency spectra for these 13 stars are shown in Fig. 8.

TIC 21018674 (= UCAC4 713-059112,  $V_{\text{mag}} = 13.36$ ): There is a pair of signals at  $1.0736$  and  $1.4385 \text{ d}^{-1}$  with  $f_{\text{rot}}$  at  $0.6649 \text{ d}^{-1}$ , and some nearby lower-amplitude signals. All confidently originate on target.

TIC 26434309 (= HD 281171,  $V_{\text{mag}} = 11.33$ ): The group of frequencies centred near  $3.2 \text{ d}^{-1}$  (the two strongest of which are  $3.10$  and  $3.23 \text{ d}^{-1}$ ) originate on target.

TIC 34366540 (= TYC 4765-708-1,  $V_{\text{mag}} = 10.63$ ): There is a signal at  $2.83 \text{ d}^{-1}$ , plus its lower-amplitude harmonic. There



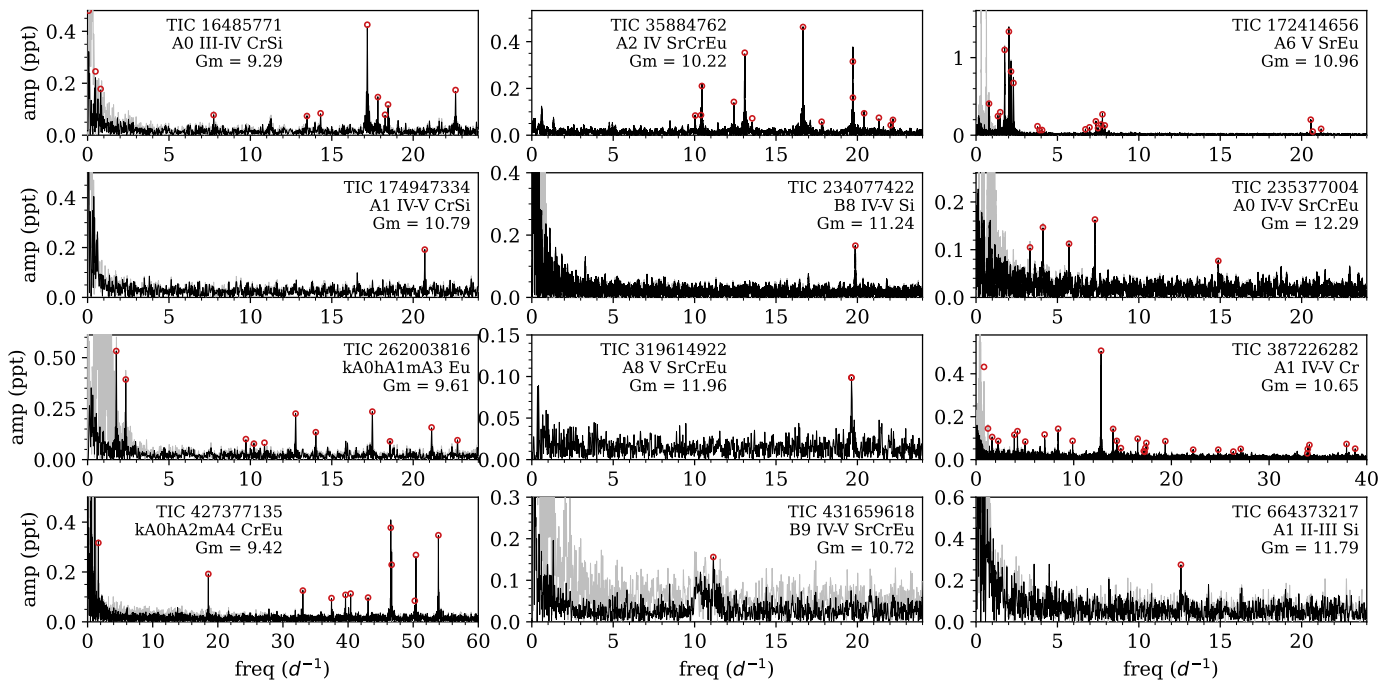


**Fig. 7.** Frequency spectrum before (lighter grey) and after (black) detrending against the rotational modulation (and in some cases low-frequency systematics) for the 12 stars with higher-frequency signals ( $>10\text{ d}^{-1}$ ). The red circles mark frequencies detected in a manual *Period04* analysis. TIC identifiers, the spectral type from Paper 1, and the *Gaia* magnitude are given in each panel.

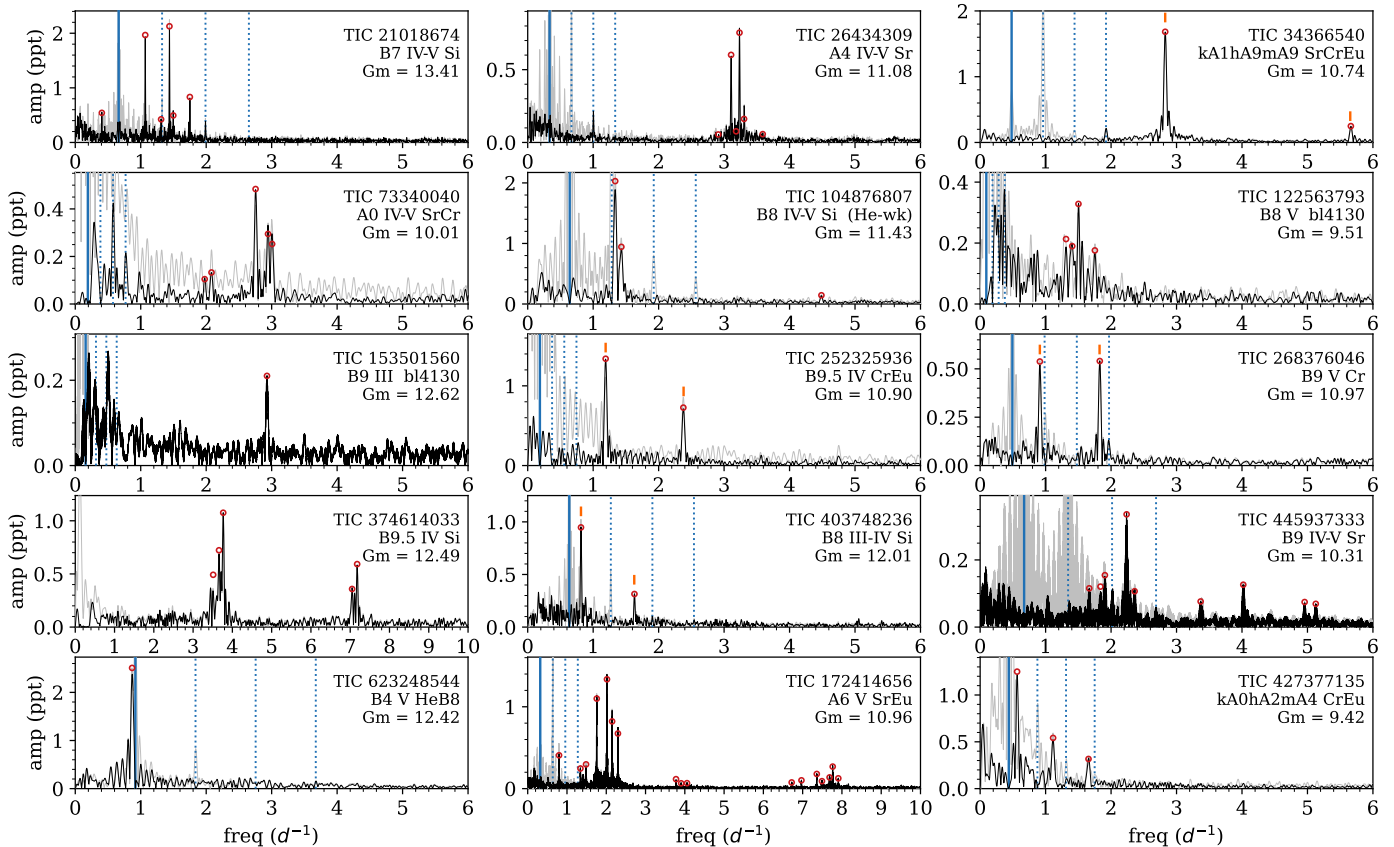


**Fig. 8.** Similar to Fig. 7, but for the lower-frequency signals ( $<10\text{ d}^{-1}$ ). The rotational frequency is indicated by a vertical solid blue line, and its first three harmonics as dotted lines. TIC 172414656 and 427377135 are also plotted in Fig. 7, but here the low-frequency regime is emphasised. Red circles mark frequencies not related to the mCP star rotation. Frequencies that form a harmonic pair are marked with a vertical orange dash.



## Appendix A: Essential data for our sample stars

Table A.1 lists essential data for our sample stars. It is organised as follows. Positional information was taken from *Gaia* DR3. Table A.1 is available in electronic form at the CDS via anonymous ftp to cdsarc.cds.unistra.fr (130.79.128.5) or via <https://cdsarc.cds.unistra.fr/cgi-bin/qcat?J/A+A/>.

- Column 1: TIC identifier.
- Column 2: LAMOST identifier.
- Column 3: Right ascension (J2000).
- Column 4: Declination (J2000).
- Column 5: Gaia magnitude,  $G_{\text{mag}}$  (Gaia DR3).
- Column 6: Spectral type from Paper 1. As in the Renson & Manfroid (2009) catalogue and Paper 1, the 'p' denoting peculiarity was omitted from the spectral classifications.
- Column 7: Period from TESS, given to the last significant digit.
- Column 8: Amplitude from TESS.
- Column 9: Remark. When available, information on variability type and period from the VSX are provided in parentheses. We note that for several objects, the VSX designations are not accurate, for example when variability was interpreted as being related to binarity and not rotation or when the object was included under a generic variability type such as ROT or MISC. These objects are here identified as ACV variables for the first time.

































## Appendix B: Correlations

For the sample of 720 stars with accurately determined photometric variability in TESS data, various correlations were explored between the TESS-derived rotational periods and photometric peak-to-peak amplitudes and stellar properties such as the absolute *Gaia* magnitude  $G_{\text{mag0}}$  and the de-reddened *Gaia* colour index  $(BP - RP)_0$ , which were both taken from Paper 1. Linear regression analysis was employed to test the statistical significance of the correlations. The results are illustrated in Fig. B.1.

Statistically significant positive correlations are found between period and colour and magnitude, and a negative correlation between period and amplitude. A weak, but not statistically significant, negative correlation is found between amplitude and colour. Since colour is a proxy for temperature, it depends on both stellar mass and age, and likewise for absolute magnitude, which depends on radius and temperature. Therefore, these correlations (or lack thereof) are not straightforward to interpret because the sample spans a wide range in mass ( $\sim 1.5$  to  $\sim 4.5 M_{\odot}$ ) and fractional main-sequence age (from the zero-age main sequence to the terminal-age main sequence).

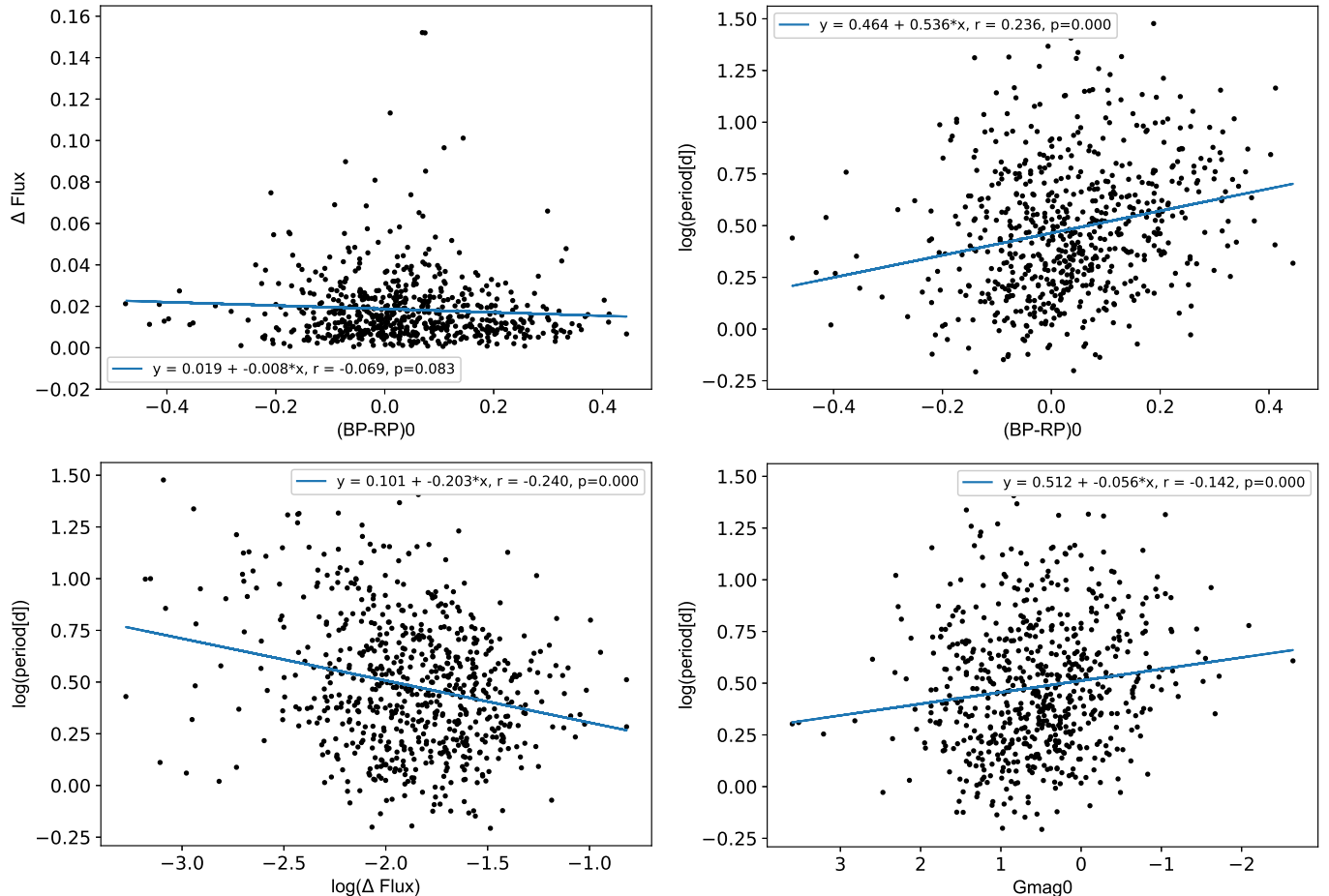


**Fig. B.1.** Correlations between several observables for the sub-sample of 720 stars with accurately determined photometric variability in TESS data. The panels investigate photometric peak-to-peak amplitude versus de-reddened colour index  $(BP - RP)_0$  (upper-left panel), logarithmic distribution of rotation periods versus de-reddened colour index  $(BP - RP)_0$  (upper-right panel), logarithmic distribution of rotation periods versus logarithmic photometric peak-to-peak amplitude (lower-left panel), and logarithmic distribution of rotation periods versus intrinsic absolute magnitude in the *G* band (lower-right panel). The blue lines illustrate a linear regression fit to the data. Coefficients and p values from the regression analysis are indicated in the insets.

Additionally, many different spectral peculiarities are represented in the sample. There are first hints of different trends and correlations between parameters for different chemical peculiarity sub-types. However, investigating this properly requires a larger sample and also a more careful determination of both the fundamental stellar properties and the chemical peculiarity classifications, which are beyond the scope of this work.